JET–P(97)48

Identification of External Kink Modes in JET

G Huysmans, T Hender[1], B Alper.

JET Joint Undertaking, Abingdon, Oxfordshire, OX14 3EA,

[1]UKAEA/Euratom Fusion Association, Culham, Abingdon, Oxfordshire, OX14 3DB, UK.

Preprint of a Paper accepted for publication in Nuclear Fusion

December 1997

ABSTRACT

The ‘Outer Mode’ is one of the MHD modes which limits the fusion performance of the hot-ion H-mode discharges in JET. Previously it was proposed that the outer mode is a non-linearly saturated external kink mode. This was based on the localisation of the perturbation close to the edge as observed in the Soft X-ray (SXR), the electron temperature and the electron density measurements. Also, MHD stability calculations showed that the plasma edge is close to the ideal external kink stability boundary at the time when the outer mode is observed. In this paper, we compare the SXR data of the outer mode with predictions based on the mode structure of the ideal n=1 external kink mode. Excellent agreement is found confirming the identification of the outer mode as an external kink mode.

1. INTRODUCTION

The hot-ion H-mode is one of the operating regimes to attain high performance (i.e. high neutron yield) in JET [1]. In this regime an initially low density target plasma is heated with substantial neutral beam power (>15 MW); the low target density allows good beam penetration to the plasma core and gives rise to a long ion-electron equipartition time, so that the ions become substantially hotter than the electrons (typically T_i ~ 20-30 keV and T_e ~10-15 keV). Since the ions are the fusion species $T_i > T_e$ tends to optimise the neutron yield for a given stored energy. As the hot-ion regime is established in a divertor configuration with significant heating power the H-mode is accessed and ELMs can occur. The highest performance is achieved by stabilising the ELM by use of moderately high triangularity plasmas (δ ~ 0.3-0.4). The ELM-free period is however transient and is almost always terminated by an MHD event as discussed in [2]. This MHD event may originate in the plasma core (sawtooth or fishbone) or at the plasma edge (giant ELM or ‘outer mode’). Discussion of the origin of the so-called outer mode is the subject of this paper.

Experimentally the outer mode is observed in Soft X-ray (SXR) data, the fast Electron Cyclotron Emission (ECE) data, the reflectometer data and the magnetics (Mirnov coils). The toroidal mode number is usually n=1 but higher n (2, 3 and 4) have also been observed. The frequency of the mode corresponds to the plasma rotation frequency near the plasma edge. For an n=1 mode the frequency is typically 10 kHz. The outer mode is localised in the outer 20% of the plasma (hence its name). Although the mode is confined to the plasma periphery the outer modes cause a global degradation of energy confinement. An example of how the outer mode can affect confinement is shown in Fig.1. In this particular case the outer mode which appears at t=12.8 s, disappears at t=13.1 s when an ELM occurs and the plasma recovers. More commonly the outer mode is followed by a giant ELM which ends the good confinement phase.

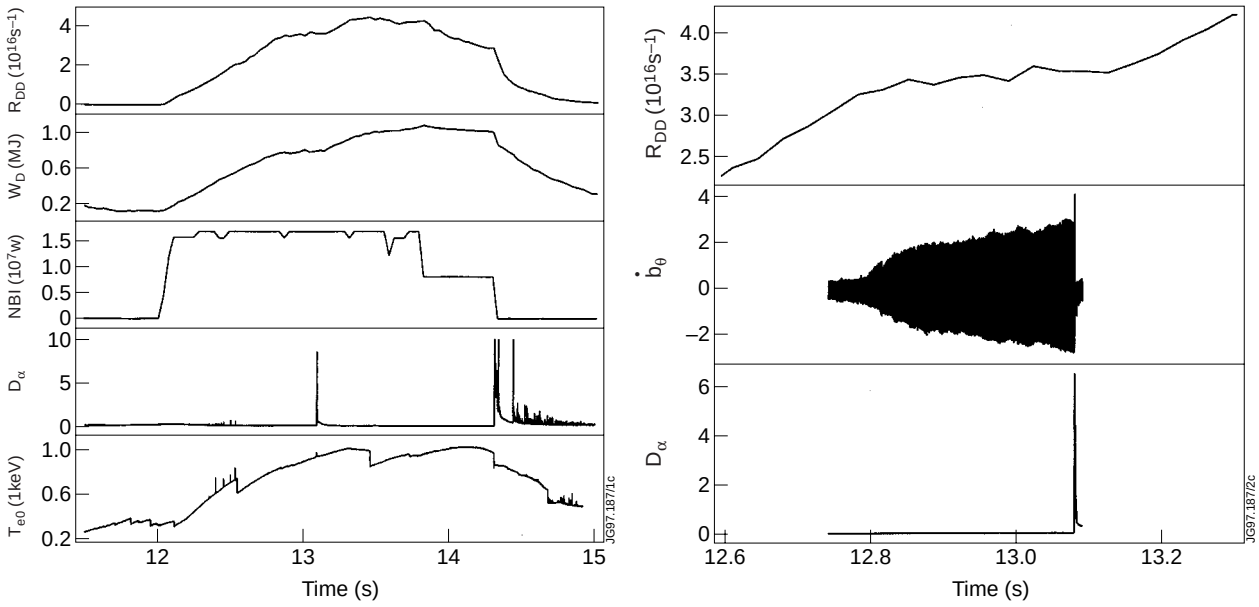

Fig.1: (a)The D-D reaction rate (R_{dd}), the stored energy (W), the neutral beam power (NBI), the D_α signal and the central electron temperature (Te_0) showing the effect of the outer mode between 12.8 and 13.1s. (b) Expanded time trace showing the outer mode growth on an outboard mid-plane Mirnov coil.

2. MHD STABILITY OF THE PLASMA EDGE

The pressure profile during a hot-ion H-mode is characterised by a large pressure gradient at the plasma edge (the edge pedestal). This edge pressure gradient leads to a significant bootstrap current. Also the high edge temperatures contribute to a significant Ohmic current density near the plasma edge, which in turn can drive an external kink mode unstable [3]. Here we analyse the MHD stability of the JET hot-ion H-mode discharge 38675 which is very similar to 38674 (shown in Fig. 1).

The profiles of the total pressure and the toroidal current density are obtained from a simulation of this discharge with the transport code JETTO [4]. The equilibrium profiles at the time when the outer mode is present at t = 13.0 s are shown in Fig.2. The plasma shape is obtained from the EFIT [5] reconstruction of the equilibrium flux surfaces using the magnetic measurements. The equilibria are recalculated using the HELENA [6] equilibrium code which provides the input for the MISHKA1 [7] ideal incompressible MHD stability code. To avoid the singular behaviour of the straight field line co-ordinate system used

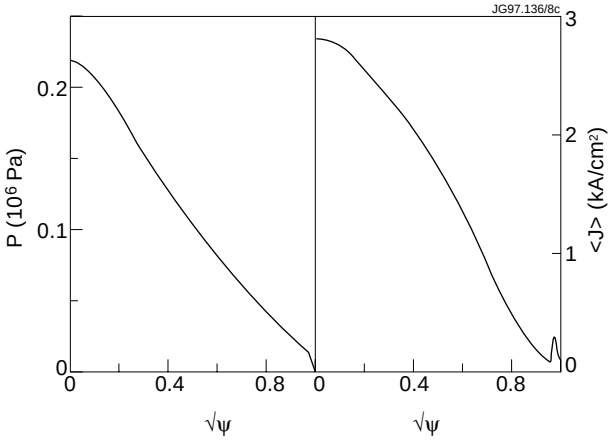

Fig.2: The pressure profile and the current density profile from the JETTO simulation of discharge 38675 at the time when the outer mode is present, t=13.0s.

in the MISHKA code at the separatrix, the plasma boundary is approximated by the ψ=0.99 surface (ψ is the normalised poloidal flux, ψ=0 on the magnetic axis, ψ=1 at the separatrix).

The stability limits of the n=1 external kink mode and the ballooning stability limit are plotted in Fig.3 as a function of the edge pressure gradient and the edge current density. The normalised pressure gradient is defined as $\alpha = -2\left(q^2 R_0 / aB_0^2\right) dp/ds$, where p is the pressure, q is the local value of the safety factor, s = $\sqrt{\psi}$, a the minor radius, R_0 the major radius and B_0 the vacuum magnetic field in the geometric centre. The stability boundaries are obtained by calculating the kink and ballooning stability of a class of equilibria with constant poloidal β_p=0.52 and constant q at the boundary while varying the edge pressure gradient and the edge current between 0.95 <ψ < 1.0. Included in the figure is the time trace of the edge pressure gradient and current density obtained from the transport code's interpretation based on experimental data. The error bars on the edge pressure gradient and the related edge current density are significant. For example, the pressure at the top of the pedestal is typically reproduced within 20%. There is no direct measurement of the edge current density, it results from the calculated neoclassical bootstrap and Ohmic currents. The pressure gradient is well below the ballooning limit while the edge current density becomes large enough to drive the n=1 external kink mode unstable. The occurrence of the outer mode when the plasma edge is close to the kink stability limit combined with the localisation of the outer mode close to the plasma boundary was previously used to identify the outer mode as an external kink mode [3]. In section 4 the mode structure of the n=1 external kink mode is compared in detail with the SXR observations of the outer mode.

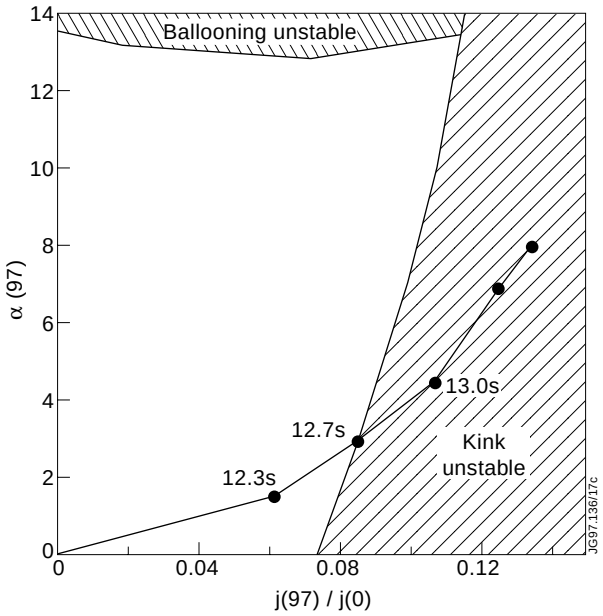

Fig.3: The edge stability diagram for discharge 38675 showing the kink and ballooning stability limits in the edge pressure gradient - edge current density plane. The pressure gradient and the current density are taken at the ψ=0.97 flux surface. Included is the time trace of the edge plasma parameters of discharge 38675.

3. THE JET SXR SYSTEM

The soft X-ray detector system used in this analysis is fully described in reference [8]. It consists of 197 lines-of-sight in 10 arrays at one toroidal location (labelled A-J and V) as shown in Fig. 4. The plasma is viewed through beryllium windows which filter out X-rays with energies below 2 keV. The diodes start to become transparent to X-rays at energies above ~10keV.

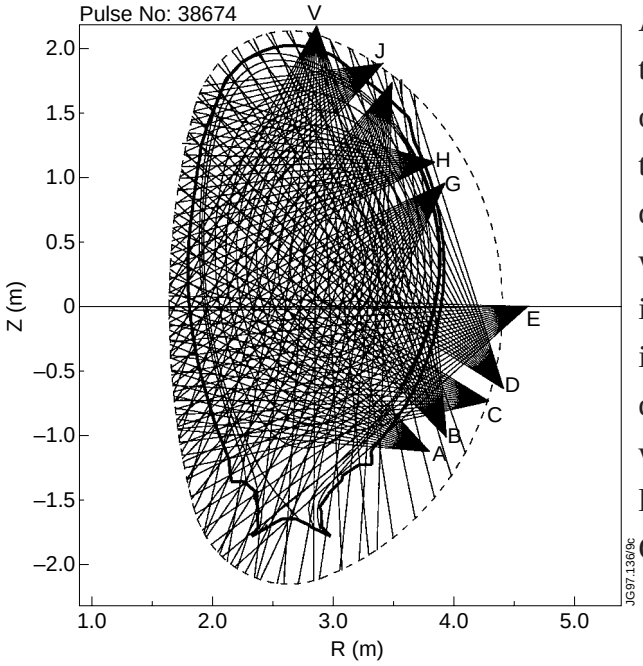

Fig.4: The JET Soft X-ray system showing the 197 lines of sight for the cameras A to J and camera V.

Another single array of 35 lines-of sight identical to array V but displaced toroidally by 3 octants(i.e. 135 degrees apart) is used for toroidal mode number (n) determination. The data is sampled at 4μs intervals with a bandwidth cut-off above 100kHz. Electronic noise is generally low and can be neglected at intensities above 80W/m^2 which applies to the data discussed here. The SXR data together with ECE and reflectometer signals are collected and processed through 'CATS' - the JET Central Acquisition and Trigger System [9].

4. COMPARISON SXR DATA WITH CALCULATED MODE STRUCTURES

In this section we compare the SXR data of the outer mode with predictions based on calculated mode structures. In sections 4.1 and 4.2 the phase of the SXR data is compared to the predictions based on an ideal external kink mode and a tearing mode respectively. In section 4.3 the absolute amplitude of the outer mode is compared with predictions based on the ideal external kink mode.

4.1 Ideal external kink mode comparison

To calculate the predictions of the SXR signals due to the ideal external kink mode, the kink mode displacements (see Fig.5a) are added to the equilibrium flux surfaces. This yields perturbed flux surfaces with an n=1 perturbation in the toroidal direction (see Fig.6). It is assumed that a given SXR emissivity profile 'moves' with the perturbed flux surfaces, allowing the line integrals over the lines of sight of the SXR cameras to be calculated. Assuming that the perturbed plasma rotates toroidally with a fixed frequency (the frequency of the outer mode), the values of the line integrals at different toroidal angles can be translated into a time dependent signal. Thus, the external kink mode is assumed to be saturated at a fixed amplitude in time and the time variation comes from the toroidal rotation of the n=1 structure.

For the first comparison, we analyse the JET discharge 37431 where a large amplitude outer mode occurs just before a giant ELM. The toroidal mode number of this outer mode, n=1, is determined from an array of 10 magnetic pick-up coils equally spaced in the toroidal angle. The phase difference between the signals of the two SXR cameras separated by 135 degrees

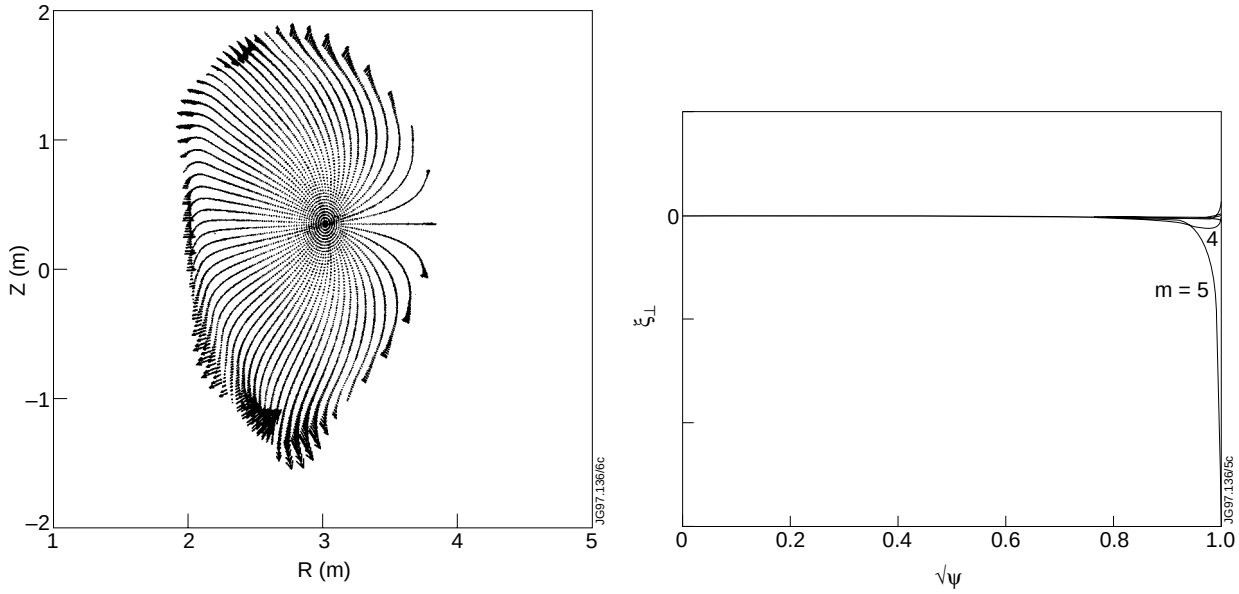

Fig.5: (a) The mode structure of the n=1 external kink mode. Shown is the perpendicular component of the displacement of the perturbation in the poloidal plane. (b) The Fourier harmonics of the n=1 external kink mode as a function of radius.

toroidally is consistent with the *n*=1 mode number obtained from the magnetics. The calculated mode structure of the *n*=1 external kink mode is shown in Fig.5, the SXR channels in which there is a clear signal due to the outer mode are plotted in Fig.6. The value of q at the boundary truncated at ψ=0.99 is just below 5 yielding a dominant poloidal mode number of *m*=5. Figure 5 shows the component of the displacement perpendicular to the flux surfaces in the poloidal plane and the Fourier harmonics of this displacement component as a function of the radius. The large poloidal component of the displacement is not shown in Fig.5. This component is parallel to the flux surfaces and will not contribute to the SXR perturbations. The external kink mode is characterised by convective cells with a large poloidal extent on the outboard side and poloidally localised structures around the x-point, where the amplitude of the mode is largest. The emissivity profile was chosen to be a constant between $0 < \psi < 0.98$; detailed comparisons shows the phase of the SXR signals does not depend sensitively on the shape of the emissivity profile. The SXR emissivity profile is cut off at ψ=0.98 to prevent having a finite predicted signal where there is no signal in the SXR data. (The SXR

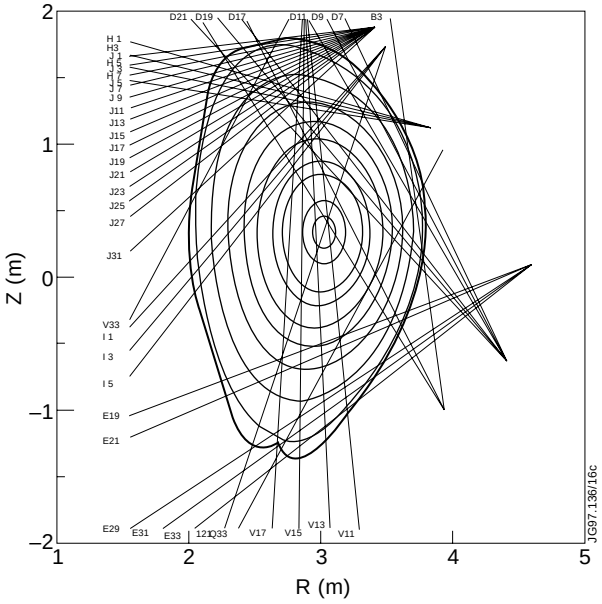

Fig.6: The perturbed flux surfaces resulting from the addition of the external kink perturbation to the equilibrium flux surfaces. Also indicated are the lines of sight of the SXR channels which 'see' the outer mode.

cameras are sensitive to energies down to 2 keV.) This means that the SXR signals arise from different chord integration lengths as the 0.98 surfaces moves.

The comparison of the normalised SXR data with the predicted values for a selection of channels is shown in Fig.7a and 7b. Figure 7a shows the SXR data and the predicted signal as a function of time for a selection of channels. In the comparison, one arbitrary constant can still be added to the phase of the predicted signals. This constant is chosen such that the phase of the E33 channel matches the SXR data. Figure.7b shows the phase of the predicted and measured signals for the 43 lines of sight which have a relatively clear outer mode signal in the SXR data. The outer mode perturbation in these channels is larger than 50 W/m^2 . The maximum amplitude of the perturbation is about 300 W/m^2, the relative amplitude varies from 25-40% in the edge channels to about 1% in the more central channels.

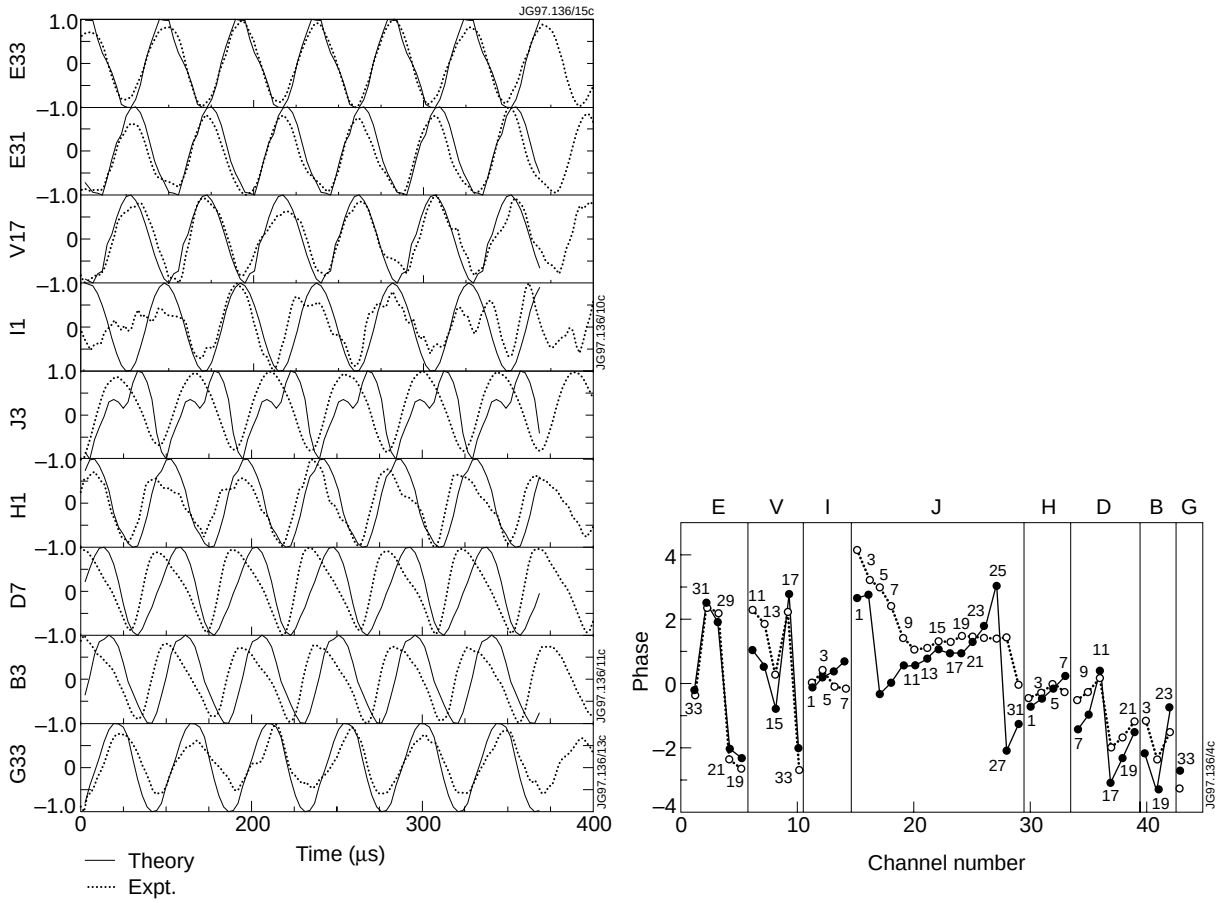

Fig.7: (a) Comparison of the SXR data (dotted lines) with the predicted signals (solid lines) based on the m=5 external kink mode. (7b) Comparison of the phases of 43 lines of sight indicated in Fig.6, the broken line is the data and the solid line the predictions.

Excellent agreement is found between the phases of the SXR data and the phase of the predicted signals. The sharp phase change of 180° between the two adjacent channels E33 and E31 observed in the SXR data is very well reproduced in the calculated phases. This phase change is due to the poloidally localised structure of the mode close to the x-point. Both

channels E31 and E33 (indicated in Fig.6) pass close to the x-point but at opposite phases of the n=1 kink perturbation. The contribution from the passage of E31/33 on the outboard side has the same phase and a smaller amplitude. The phase of the channels on the top of the plasma and on the outboard side are also well reproduced. This yields a strong confirmation that the outer mode can be identified as an external kink mode.

Due to the strong asymmetry in the mode structure with the poloidal angle it is very difficult to determine the poloidal mode number from the Mirnov coil data. One way to determine the poloidal mode number is to compare the SXR data with the external kink mode structure with different dominant poloidal mode numbers (see Fig.8). The dominant harmonic is varied by adjusting q at the boundary by changing the total plasma current. The m=4 external kink predicted signals agree less well with the SXR data. The cameras looking at the outboard side are well reproduced (cameras H, D and B) but the camera E looking at the x-point does not agree well. The m=6 mode data (Fig 8b) also does not agree as well to the data. One phase change in the predicted data on the outboard side (cameras B and D) is not observed in the SXR data. The best agreement is obtained with the m=5 external kink mode. This happens to be when the plasma boundary is approximated by the ψ=0.99 surface, q_{99} = 4.7 so that the most unstable n=1 mode has a dominant m=5 contribution.

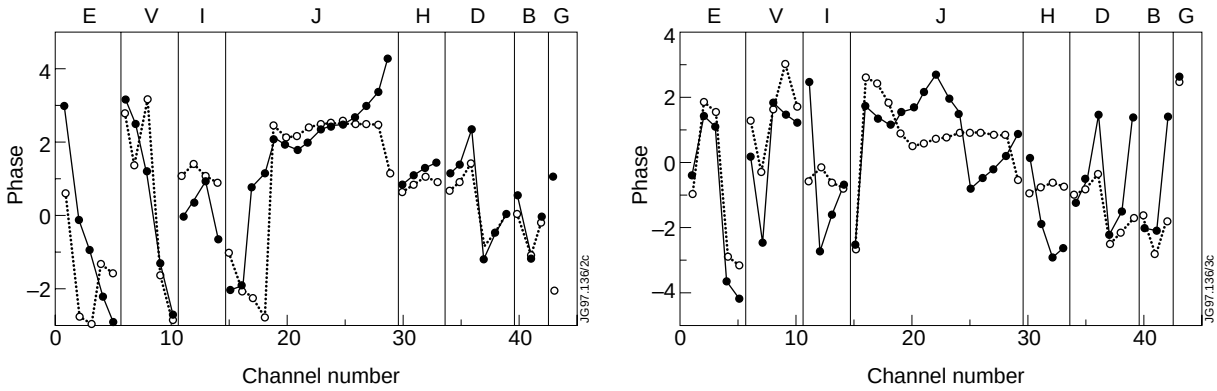

Fig.8: Comparison of the SXR data (solid lines, filled symbols) with the m=4 (a) and m=6 (b) external kink predictions (dotted line open symbols). In these figures the (arbitrary) relative phase of the data is adjusted to give the best fit to the prediction.

Next, we analyse the outer mode in discharge 38674 as shown in Fig.1. The amplitude of the outer mode is much smaller than in 37431, the maximum perturbation is now only 50 W/m^2. Consequently, there are fewer channels which show a relatively clear outer mode signal. The predicted signals and the SXR data for #38674 are shown in Fig.9 for 26 channels where the outer mode is seen. Again very good agreement is found between the SXR data and the predictions based on the n=1, m=4 kink mode. A sharp phase change at the x-point similar to the one observed in #37431 shows up in the channels E31-E29. Again this is very well reproduced by the calculated phases.

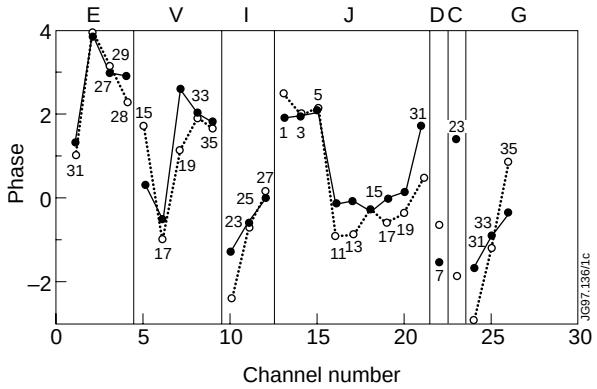

Fig.9: Comparison of the phases of the outer mode as seen in the SXR data and the phases of the n/m=1/4 kink mode for discharge #38674.

In this discharge a poloidal mode number of m=4 kink mode gives the best agreement with the SXR data. This is consistent with the higher plasma current (3.8MA compared to 3.1 MA for discharge 37431) and a lower q, close to 4., at the ψ=0.99 surface.

4.2 Tearing mode comparison

The SXR data has also been compared with predictions based on resistive tearing modes (i.e. modes which form magnetic islands) which have been computed using the toroidal resistive MHD code CASTOR [10]. The ideal external kink mode was stabilised by removing the edge current and a tearing mode was made unstable by artificially adding a large current gradient at the q=3 surface, which gives a predominantly m=3 mode. The aim here is to eliminate the possibility that this internal mode may explain the observed outer mode behaviour. For the m=5 mode described in the previous section the addition of resistivity makes no significant change to the eigenfunction structure.

For resistive modes the plasma is not 'frozen' to the MHD perturbation and a different approach is needed to calculate the SXR signals. The approach used is to assume that SXR emission is constant on any given perturbed magnetic field line and that the emission on that field line is specified as a function of its average minor radius. This leads to flattening of the emissivity profile in the o-points of the islands created by the tearing mode. The emissivity profile used is determined by a flux surface averaged tomographic reconstruction. It should be noted that while the tomographic reconstructions show the SXR emission is far from being a flux surface variable in the core [11], near the edge (where the outer mode is localised) this is a reasonable approximation. This field line calculation procedure yields the SXR values along the viewing chords, allowing the line integrals to be performed. As in Section 4.1 an equivalence between toroidal angle and time is assumed, so that the perturbed temporal SXR behaviour may be predicted. This procedure has been tested by computing the predicted SXR signals for the ideal mode (from CASTOR) and comparing with equivalent signals using the method discussed in Section 4.1; good agreement is found which validates the method.

Figure 10 shows a comparison of ideal and resistive mode predictions for a selection of SXR channels. The tearing mode has a dominant harmonic of *m*=3 and is driven unstable by the current gradient. Unlike the ideal external kink mode, the structure of the tearing mode is not sensitive to the value of q at the boundary.

From Fig. 10 it can be seen that while the ideal mode prediction gives good relative phase agreement with the data, the agreement for the resistive mode is much poorer. Since the relative

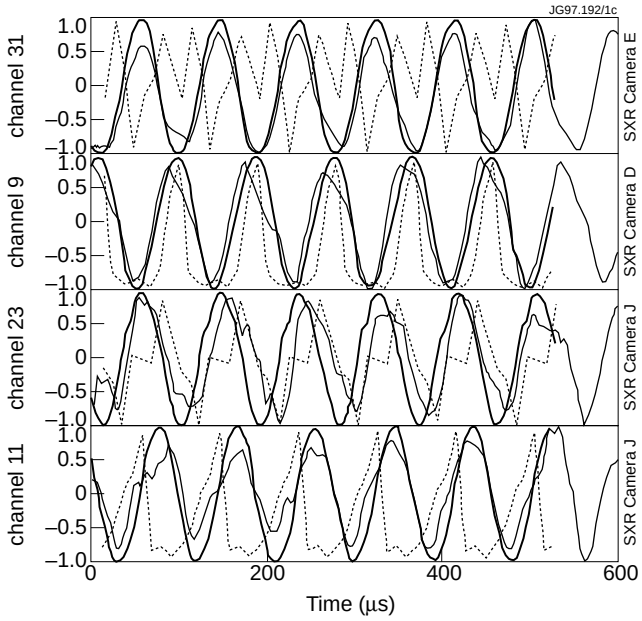

Fig.10: Comparison of SXR data (thin line) with predictions for the dominantly m=5 ideal kink mode (thick solid line) and resistive mode (broken line) for shot 37431.

phase agreement is poor no attempt at an amplitude comparison has been made for the resistive mode.

4.3 The mode amplitude

Given the good agreement found between the phases of the SXR signals and the predicted phases based on the ideal external kink mode, the same mode structure can be used to determine the absolute amplitude. By using a time averaged SXR emission profile consistent with the absolute values of the different SXR channels, the amplitude of the kink mode can be fitted to get best agreement with the perturbed SXR data.

To determine the amplitude of the external kink mode locally at the x-point where the amplitude is largest the E-camera data which views the x-point is used. Inversion of the E-camera data for discharge #37431, averaged over several periods of the perturbation, yields the local equilibrium emissivity profile as a function the flux (the local emissivity is assumed to be a function of the flux). Figure 11 shows the resulting (local) equilibrium emissivity profile and the E-camera channel data with the values calculated from the fitted equilibrium profile. The error in the fit is less then 2%.

Using this emissivity profile the predictions for the SXR channels are calculated as in section 4.1 where the amplitude of the added kink perturbation is now adjusted to give the best fit to the absolute value of the data. The results for the 3 outer most channels (closest to the x-point) are plotted in Figure 12. The agreement for the amplitude is reasonably good. Channel 31 is close to the phase change where the amplitude changes rapidly and is therefore the most difficult to fit. The resulting size of the perturbation of the flux surfaces is about 10 cm at the

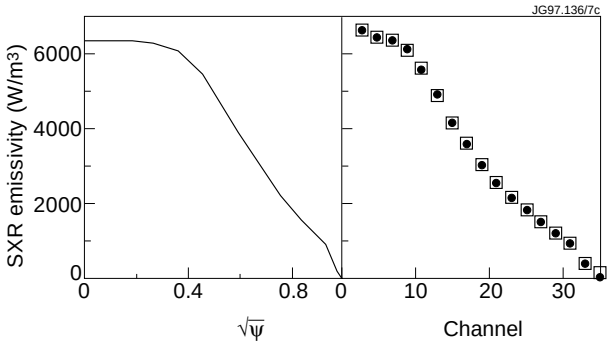

Fig.11 (a) The equilibrium SXR emissivity profile for discharge #37431. (b) The E-camera data as a function of channel number (filled circles) and the values from the fit of the equilibrium profile (open squares).

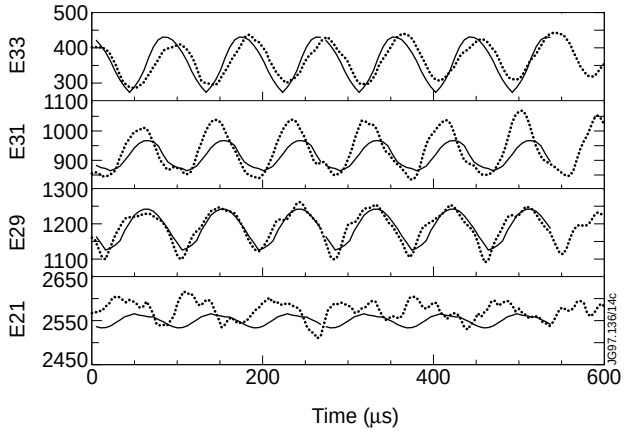

Fig.12 Comparison of the absolute amplitudes of the SXR data (line integrals of the SXR emission in W/m2, dotted line) and predictions (solid line) based on the ideal kink mode using the equilibrium emissivity profile of Fig.11.

x-point and about 1 cm at the outboard mid-plane. The amplitude of the perturbation at the x-point is well outside the error bars of the position of the x-point of 1-2 cm as determined by the EFIT equilibrium reconstruction. The value at the outboard midplane is slightly less than estimates based on the ECE electron temperature data [2]. Figure 6 shows the perturbed flux surfaces with the actual size perturbation.

5. CONCLUSIONS

The outer mode is one of a range of instabilities which can limit performance for hot ion H-modes discharges in JET. Stability calculations indicate that the ideal external kink mode becomes unstable (within experimental error bars) when the outer mode is observed. The results presented in this paper, showing excellent phase and amplitude agreement between SXR data and predictions based on the ideal external kink mode, provide very strong evidence on the cause of the outer mode. Equivalent comparisons for the m=3 resistive kink mode show poor agreement with outer mode SXR data. This identification of the outer mode as being a current driven instability suggests means for its control (by reducing the edge current density). Initial experiments using modest ramp-downs in the plasma current (to reduce the edge current density) have been successful in delaying the outer mode, indicating the value of a good physics understanding of this instability.

ACKNOWLEDGEMENTS

The UKAEA author was jointly funded by the UK Department of Trade and Industry and Euratom. We thank P. Smeulders for the initial suggestion to compare the calculated mode structures with the SXR data. We thank V. Parail for the use of JETTO simulation data.

REFERENCES

[1] The JET team, Plasma Phys. Control. Fusion **37** (1995), p. A359.
T.T.C. Jones and the JET team, Phys. Plasmas **4**, No. 5 (1997), p.1725.

[2] NAVE F., et al., Nuclear Fusion Vol. 37, No. 6 (1997) p. 809.

[3] HUYSMANS G.T.A., CHALLIS C.D., ERBA M., KERNER W. and PARAIL V.V., 22nd EPS Conf. on Controlled Fusion and Plasma Physics, Bournemouth 1995, (Ed. B.E. Keen, P.E. Stott and J. Winter, publ. European Physical Society, 1995), Vol.19C, p. I-201.

[4]. CHERUBINI A., ERBA M., PARAIL V., SPRINGMANN E., and TARONI A., Plasma Phys. Control. Fusion **38** (1996) p.1421.

[5] LAO L., et al. , Nucl. Fusion **30** (1990), p.1035.

[6] HUYSMANS G.T.A., GOEDBLOED J.P., and KERNER W.O.K., CP90 Conf. on Comp. Physics Proc., World Scientific Publ. Co.,(Ed. A. Tenner) 1991, p.371

[7] MIKHAILOVSKII A.B., HUYSMANS G.T.A., KERNER W.O.K., SHARAPOV S.E., Plasma Phys. Rep., Vol. 23, No. 10, p.844 (1997).

[8] ALPER B., et al, Rev. Sci. Instr. **68**, 778 (1997).

[9] BLACKLER K. and EDWARDS A. W., IEEE Trans. Nucl. Sci. **41**, 111 (1994).

[10] KERNER W.O.K., GOEDBLOED J.P., HUYSMANS G.T.A., POEDTS S. and SCHWARTZ E., 'CASTOR: Normal Mode Analysis of Resistive Plasmas', JET Report JET-P(97)04, submitted for publication in Journal of Computational Physics.
HUYSMANS G.T.A., GOEDBLOED J.P. and KERNER W., Phys. Fluids B, **5**, (1993), p.1545.

[11] ALPER B., et al., 23rd EPS Conf. on Contr. Fusion and Plasma Physics, Kiev 1996, (ed. D Gresillon, A. Sitenko and A. Zagorodny, publ. European Physical Society, 1996), Vol.20C, part I, p.163.